IEEE Photonics Journal
An IEEE Photonics Society Publication

Open Access

Design and Analysis of a Miniature Intensity Modulator Based on a Silicon-Polymer-Metal Hybrid Plasmonic Waveguide

Volume 6, Number 3, June 2014

Xiaomeng Sun
Linjie Zhou, Member, IEEE
Haike Zhu
Qianqian Wu
Xinwan Li, Senior Member, IEEE
Jianping Chen, Member, IEEE

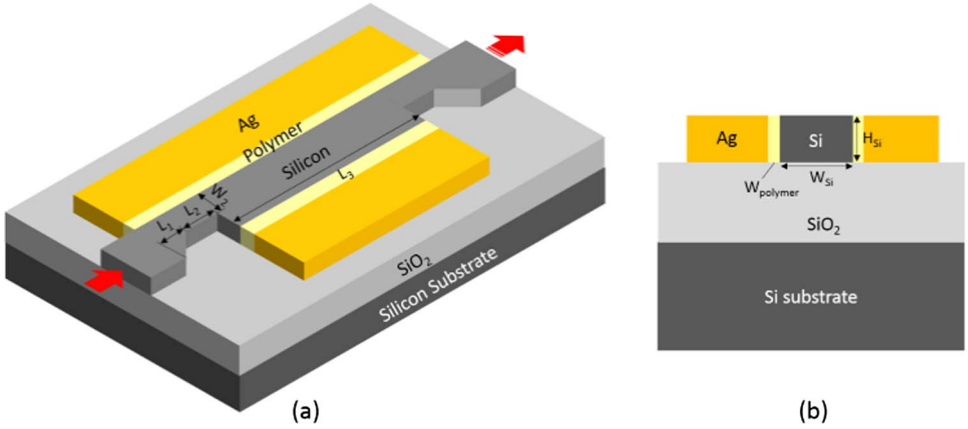

DOI: 10.1109/JPHOT.2014.2329395
1943-0655 © 2014 IEEE

Design and Analysis of a Miniature Intensity Modulator Based on a Silicon-Polymer-Metal Hybrid Plasmonic Waveguide

Xiaomeng Sun,[1,2] Linjie Zhou,[1] *Member, IEEE*, Haike Zhu,[1] Qianqian Wu,[1] Xinwan Li,[1] *Senior Member, IEEE*, and Jianping Chen,[1] *Member, IEEE*

[1]State Key Laboratory of Advanced Optical Communication Systems and Networks, Department of Electronic Engineering, Shanghai Jiao Tong University, Shanghai 200240, China
[2]Fachgebiet Hochfrequenztechnik, Technische Universität Berlin, Berlin 10587, Germany

DOI: 10.1109/JPHOT.2014.2329395

Manuscript received April 22, 2014; revised May 23, 2014; accepted May 24, 2014. Date of publication June 6, 2014; date of current version June 18, 2014. This work was supported in part by the 973 Program under Grant ID2011CB301700 by the 863 Program under Grant 2013AA014402 by the National Natural Science Foundation of China (NSFC) under Grants 61127016 and 6110704, and by the Science and Technology Commission of Shanghai Municipality (STCSM) Project under Grant 12XD1406400 Corresponding author: L. Zhou (e-mail: ljzhou@sjtu.edu.cn).

Abstract: We propose a miniature optical intensity modulator based on a silicon-polymer-metal hybrid plasmonic waveguide. Benefiting from the high mode confinement of hybrid plasmonic waveguide and the high linear electro-optic effect of polymer material, the intensity modulator is ultra-compact with a length of only $\sim$13 μm. The device is optimized using numerical simulations based on the finite element method (FEM). The modulator exhibits a large modulation bandwidth of 90 GHz, a modulation depth of 12 dB at 6 V, and low power consumption of 24.3 fJ/bit.

Index Terms: Plasmonics, waveguide devices, silicon nanophotonics.

1. Introduction

Optical technology is able to revolutionize short-reach interconnects, ranging from high-performance computing and data centers down to mobile-to-server interconnects and desktop computers [1]. Optical interconnects could bring several major advantages over their electrical counterparts, such as higher bandwidth, fewer physical layers, less transmission loss and power consumption, weaker electromagnetic interference, shorter cable length and smaller cable weight. The leading candidate technology in optical interconnects is silicon photonics, of which one of the most important building blocks is the optical modulator. Optical modulators can be categorized into amplitude, phase, and polarization modulators. Modulation speed, modulation depth, power consumption, operation spectral window, insertion loss, and device footprint are the key device parameters to measure the modulation performance.

Many materials can be used for optical modulators, such as III-V compounds, lithium niobate ($LiNbO_3$), silicon, germanium or silicon-germanium (Ge/SiGe) quantum well, and polymer. Strained Ge/SiGe quantum well with relatively strong electro-optic absorption due to quantum-confined Stark effect is an excellent candidate for optical modulators [2]. However, critical strain engineering is

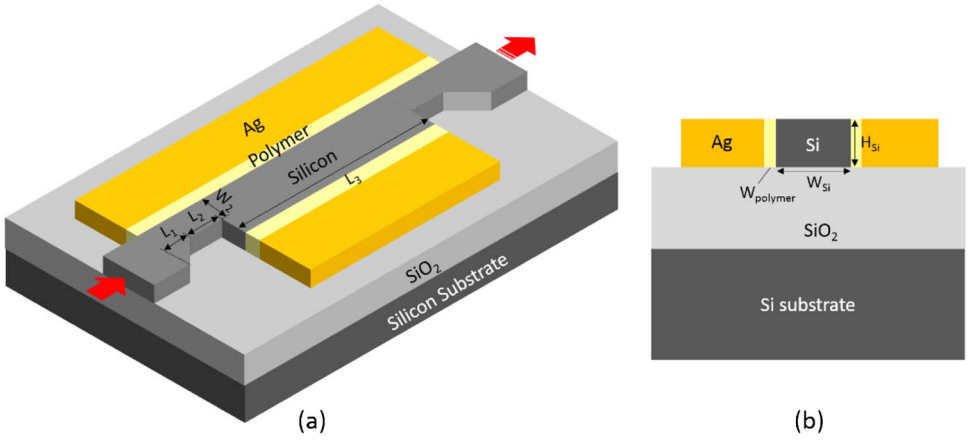

Fig. 1. (a) Schematic perspective view of the proposed optical intensity modulator. L_1, L_2, and L_3 are taper, SSHW, and DSHW lengths, respectively. (b) Cross-sectional view of the DSHW.

needed. Silicon is a well-understood semiconductor material and silicon-based modulators are complementary metal-oxide-semiconductor (CMOS) compatible, which makes them quite attractive. Various mechanisms can be utilized to implement silicon modulators, including free-carrier plasma dispersion effect [3]–[5], Kerr and Franz-Keldysh effects [6], and thermo-optic effect [7], [8]. However, refractive index change induced by the free-carrier plasma dispersion effect is relatively weak, typically on the order of 10^{-3}, which is challenging to make the modulator very compact. The Kerr and Franz-Keldysh effects are nonlinear electro-optic effects, even weaker than the free-carrier plasma dispersion effect. The thermo-optic effect is quite strong in silicon (thermo-optic coefficient $\sim 1.86 \times 10^{-4}$), but it has slow response. Polymer-based modulators possess fast modulation speed and large modulation bandwidth, but they have large device dimensions due to the low optical confinement of polymer waveguides [9], [10].

To improve the modulator performance, scaling down the modulator dimension is one feasible way. However, due to the diffraction limit, the conventional dielectric waveguides cannot be smaller than a half wavelength. In order to break the diffraction limit and confine light into a smaller volume, surface plasmon polaritons (SPPs) have recently been employed to build various integrated plasmonic devices [11]–[21]. SPP based devices, featured with high optical field confinement at the interface, are one of the most promising candidates for high-density integration.

Here, we propose an optical intensity modulator based on a silicon-polymer-metal hybrid plasmonic waveguide to realize high-speed and low-power optical modulation. The hybrid plasmonic waveguide combines the merits of both plasmonic and photonic waveguides, namely, high optical confinement, low propagation loss, and easy integration with photonic devices. Intensity modulation in the proposed modulator is achieved by mode beating between symmetric (quasi-even) and asymmetric (quasi-odd) hybrid plasmonic modes. The effective refractive indices of the hybrid plasmonic modes can be tuned by an external voltage due to the linear electro-optic effect of polymer. As the two modes experience unequal phase delays, the change in beating period results in the variation in output power. Since the modulator is based on a single hybrid plasmonic waveguide, it is more compact than a Mach-Zehnder Interferometer (MZI) modulator where two separate waveguides are necessary to enable the optical interference. It should be noted that the proposed modulator is essentially an interference structure rather than a resonance one, therefore allowing for broadband operation [22], [23].

2. Device Structure and Working Mechanism

Fig. 1(a) shows the schematic perspective view of the proposed modulator. The two silver (Ag) strips have an unequal length which is critical to realize intensity modulation. Fig. 1(b) is the cross-sectional view of the hybrid plasmonic waveguide in the central part. The device is upper-

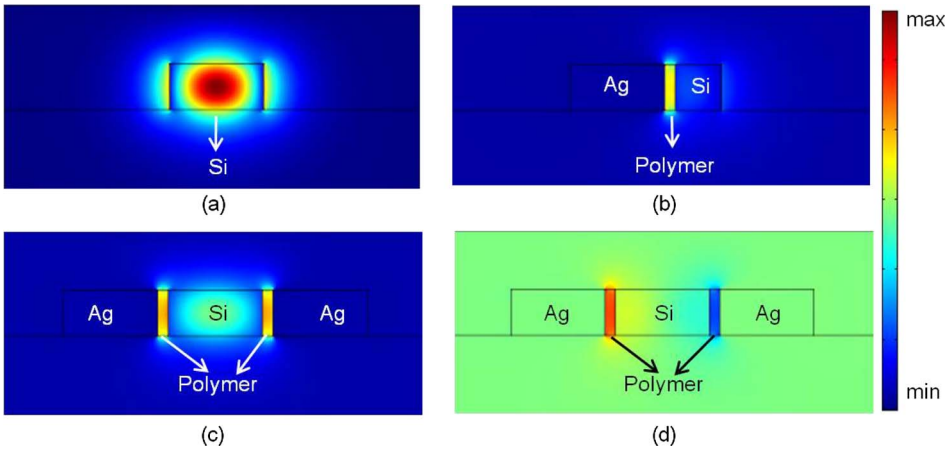

Fig. 2. Transverse electric field mode patterns for various waveguide modes: (a) Input/output silicon waveguide mode, (b) SSHW mode, (c) DSHW quasi-even mode, and (d) DSHW quasi-odd mode. $W_{Si} = 450$ nm, $H_{Si} = 250$ nm, and $W_{polymer} = 50$ nm.

clad with a silicon oxide layer (not shown in the graph). For the transverse electric (TE) polarization, the field in the polymer nano-slots is greatly enhanced due to the SPP excitation at the Ag-polymer interface and the electric field discontinuity at the Si-polymer interface [19], [20]. Nonlinear polymers are good insulating materials with a very high resistivity of 10^{11} ohm $\cdot$ cm [24]. The silver, polymer, and silicon layers form a lateral capacitor. The silicon core is intentionally n-type doped with a concentration of 3×10^{19} cm^{-3} in order to reduce its resistivity and improve the modulation speed. The doping induced free carrier absorption loss is still much smaller than the loss from the metal.

Coupling light into the hybrid plasmonic waveguide is achieved via a silicon waveguide. When light is launched at the input port, optical power is well-confined in the silicon core, as shown in Fig. 2(a). When it meets the first metal block, the optical power is gradually attracted to the slot (polymer) region of the single-slot hybrid plasmonic waveguide (SSHW), exciting the single-slot plasmonic mode as shown in Fig. 2(b). In order to reduce the mode transform loss from the dielectric to the hybrid plasmonic modes, the silicon waveguide is adiabatically tapered. At the central part where a second metal block is positioned along the other side of the silicon waveguide to form the dual-slot hybrid plasmonic waveguide (DSHW), the optical power is transferred from one slot to the other, resulting in a periodic coupling. At the end of the DSHW, light couples back to the single slot, with its coupling efficiency determined by the power distribution in the DSHW. As the optical power is strongly confined in the slots, it has a large overlap with the polymer infiltrated in the slots. Hence, the coupling length and thus the transmitted power are very sensitive to the refractive index variation in the slots. The periodic oscillation of the optical power in the DSHW is similar to that in a conventional directional coupler, except that here the slot mode coupling is radioactive rather than evanescent, leading to a much shorter coupling length.

The coupling in the DSHW can also be regarded as mode-beating between the symmetric (quasi-even) and asymmetric (quasi-odd) super-modes of the hybrid plasmonic waveguide. Fig. 2(c) and (d) show the electric field patterns of the quasi-even and quasi-odd modes in the DSHW. With a refractive index change of the polymer, the plasmonic super-modes experience different phase shifts, and therefore the interference varies at the end of the DSHW.

3. Theoretical Modeling

At the entrance of the DSHW, the input electric field $\vec{E}_1$ is expressed as

$$\vec{E}_1(x, y) = \vec{E}_s(x, y) \tag{1}$$

where $\vec{E}_s$ is the electric field of the SSHW mode. The electric field $\vec{E}_d$ in the DSHW can be decomposed into two orthogonal eigenmodes [25], and thus we have

$$\vec{E}_d(x,y,z) = C_{se}\vec{E}_e(x,y)e^{j\beta_e z} + C_{so}\vec{E}_o(x,y)e^{j\beta_o z} \tag{2}$$

where $\vec{E}_e$ and $\vec{E}_o$ are the electric fields of the quasi-even and quasi-odd modes, β_e and β_o are their complex propagation constants, and C_{se} and C_{so} are the coupling coefficients. According to the orthogonal relationship, the mode coupling coefficient C_{ij} from the i-mode to the j-mode can be calculated from the overlap integral between the SSHW and DSHW mode fields [26]

$$C_{ij} = \frac{1}{2}\iint_S \vec{E}_i \times \vec{H}_j \cdot \hat{z}\, dS \tag{3}$$

where S is the infinite cross-section, $\hat{z}$ is the unit vector in the propagation direction. The fields are all normalized. After the beating section, light is partially coupled back to the SSHW with the electric field $\vec{E}_2$ expressed as

$$\vec{E}_2(x,y) = (C_{es}C_{se}e^{j\beta_e L} + C_{os}C_{so}e^{j\beta_o L})\vec{E}_1(x,y). \tag{4}$$

The beating between the quasi-even and quasi-odd eigenmodes results in optical power oscillation between the two slots. The coupling length is given by $L_c = \pi/|\beta_e - \beta_o|$. After even numbers of coupling lengths, the power is coupled back to the single slot leading to the maximum transmission.

4. Numerical Analysis

We use a commercial finite-element simulation package COMSOL to analyze the performances of the proposed optical intensity modulator [18], [27], [28]. In our simulation, silver is assumed to have a permittivity $\varepsilon_{Ag} = -133.75 + 3.337i$ around 1550 nm wavelength [29]. Refractive indices for SiO_2, Si, and polymer are $n_{SiO2} = 1.46$, $n_{Si} = 3.48$, and $n_{polymer} = 1.6$, respectively. We use molecular glasses based on the reversible self-assembly of aromatic/perfluoroaromatic (Ar-ArF) dendron-substituted nonlinear optical (NLO) chromophores as the electro-optic polymer to actively tune the hybrid plasmonic mode. The polymer has an electro-optic coefficient r_{33}>200 pm/V with good alignment stability [30]. The polymer refractive index change Δn to an external electric field E is given by [10]

$$\Delta n = -r_{33}n_{polymer}^3 V/2W_{polymer} \tag{5}$$

where V is the voltage applied on the polymer layer.

4.1. Hybrid Plasmonic Mode

For dielectric waveguides, light is confined in the high-index dielectric layers due to total internal reflection. However, for the hybrid plasmonic waveguides, the intensity maxima are located in the low-index sidewall polymer layers for TE polarization. When the core width W_{Si} is small (< 200 nm), the DSHW can only support one mode, with its major electric field evenly distributed in the two nano-slots (quasi-even mode). When W_{Si} increases, the mode with its major electric field opposite in the two nano-slots (quasi-odd mode) shows up, which means $W_{Si} = 200$ nm is the cutoff width for the odd mode. The DSHW can be regarded as a coupled hybrid SPP system with its mutual coupling enabled through the central silicon core. The mutual coupling results in mode splitting into even and odd polarities. The complex effective refractive index of the hybrid plasmonic waveguide mode can be expressed as $n_{eff} = n_{re} + in_{im}$, where n_{re} and n_{im} are associated with light propagation

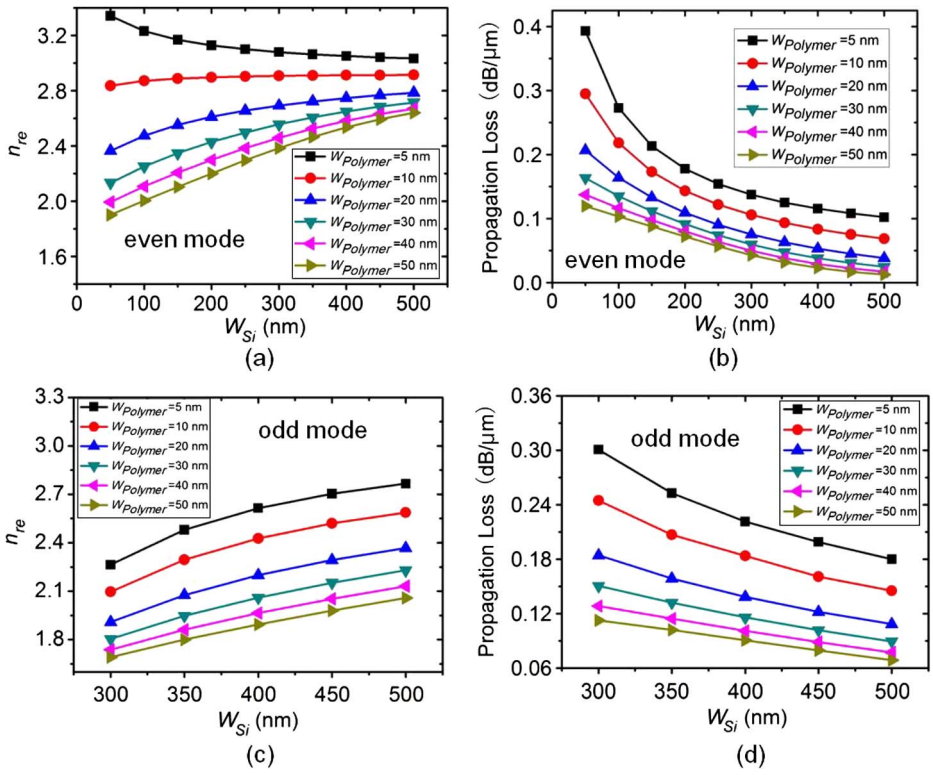

Fig. 3. (a) and (c) Real part of the quasi-even and quasi-odd modes as a function of W_{Si}. (b) and (d) Propagation loss of the quasi-even and quasi-odd modes as a function of W_{Si}.

constant and loss, respectively. The propagation loss is given by $20\lg(e)k_0 n_{im}$ [19], where k_0 is the free space propagation constant.

Fig. 3(a) and (c) show n_{re} of the quasi-even and quasi-odd modes as a function of silicon width W_{Si}. It can be seen that for the quasi-even mode, n_{re} decreases with W_{Si} when the polymer layer is thin (e.g., 5 nm), but increases with W_{Si} when the polymer layer is thick. For the quasi-odd mode, n_{re} always increases with W_{Si}. n_{re} of the quasi-even mode is larger than that of the quasi-odd mode, because it has more power distributed in the silicon core. For a given W_{Si}, n_{re} becomes larger for a thinner polymer layer. Note that when the polymer layer is very thin and less than a critical value, the field in the slots is greatly enhanced and the metal-polymer-silicon stack at each side can independently support a hybrid SPP mode with $n_{re} > n_{si}$ (for example, n_{re} can reach 3.9 when the polymer and silicon layers are 2 and 50 nm thick, respectively) [31]. When W_{Si} increases, optical power of the quasi-even mode is gradually pushed to the silicon core from the low-index sidewall polymer. Fig. 3(b) and (d) show the associated propagation loss as a function of W_{Si}. For a given W_{Si}, the propagation loss is higher for a narrower polymer layer due to the high optical field at the Ag-polymer interface.

4.2. Coupling Length

Fig. 4(a) shows the effective refractive index difference $\Delta n_{re} = n_{re(even)} - n_{re(odd)}$ between the quasi-even and quasi-odd modes as a function of W_{Si}. It can be seen that for a thick polymer layer, Δn_{re} first increases and then decreases with W_{Si}. For a thin polymer layer, Δn_{re} always decreases with W_{Si}. Interestingly, Δn_{re} is almost independent of $W_{Polymer}$ when $W_{Si} = \sim$350 nm, which means the refractive indices of both modes have a comparable change with the varying polymer width. Fig. 4(b) shows the corresponding coupling length L_c given by $L_c = \pi/|\beta_e - \beta_o| = \lambda/(2\Delta n_{re})$, which is inversely proportional to Δn_{re}. As shown in Fig. 4(b), the coupling length is very short, making it possible to realize an ultra-compact optical modulator.

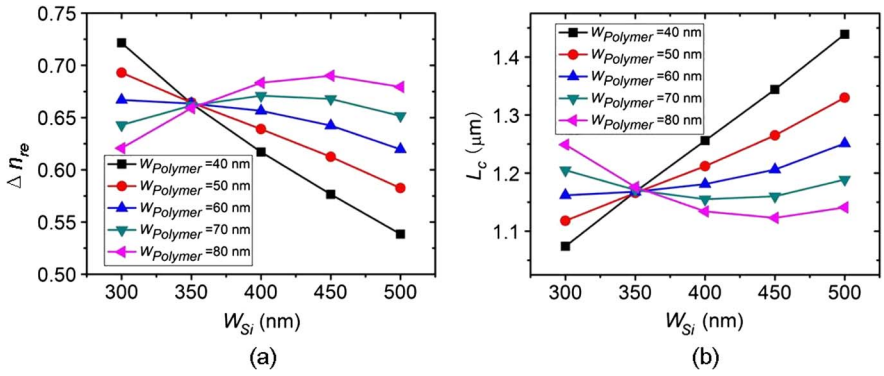

Fig. 4. (a) Effective refractive index difference Δn_{re} between the quasi-even and quasi-odd modes as a function of W_{Si}. (b) Coupling length L_c as a function of W_{Si}.

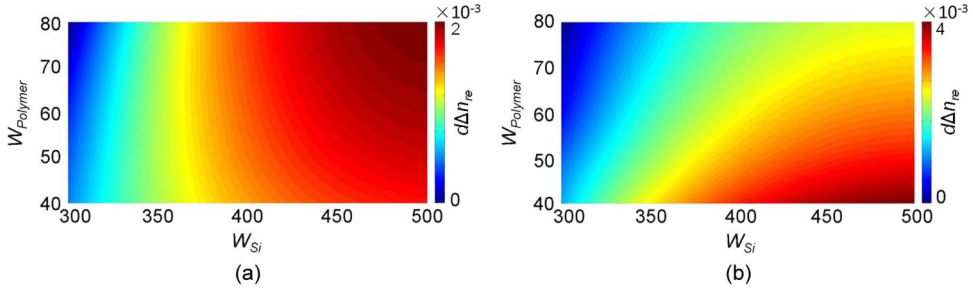

Fig. 5. Increment of the effective refractive index difference $(d\Delta n_{re})$ between the quasi-even and quasi-odd modes as a function of W_{Si} and $W_{polymer}$ when (a) the polymer refractive index change is fixed at $dn_{poly} = -0.005$ and (b) the applied voltage is fixed at $V_d = 1$ V.

4.3. Sensitivity

Sensitivity of the refractive index difference to the polymer index variation is the key parameter that determines the modulation depth and power consumption. With a voltage applied onto the hybrid plasmonic waveguide, the refractive indices of both modes are changed due to the linear EO effect of polymer. Because of their distinct mode profile, their index change is different. As a result, the quasi-even and quasi-odd modes experience different phase delays, leading to an intensity modulation at the output waveguide. Here, we define the sensitivity as

$$S \equiv \frac{d\Delta n_{re}}{dn_{poly}} = \frac{dn_{re(even)}}{dn_{poly}} - \frac{dn_{re(odd)}}{dn_{poly}}. \tag{6}$$

Fig. 5(a) shows the contour plot of $d\Delta n_{re}$ as a function of W_{Si} and $W_{polymer}$. The polymer refractive index change is assumed to be $dn_{poly} = -0.005$ in both slots. In our study, we assume that the modulator works in the synchronous mode, which can be guaranteed in practice by properly poling the polymer in the two slots. It can be seen that a wide silicon core and a thick polymer layer help to improve the sensitivity. However, it should be noted that a higher voltage is needed for a thicker polymer layer to reach the same index change. Fig. 5(b) shows the contour plot of $d\Delta n_{re}$ when the applied voltage is fixed at $V_d = 1$ V. As we can see, the polymer layer should be thin and the silicon core should be wide in order to improve the sensitivity.

4.4. Modulation Depth

The silicon core gradually narrows down at the input and output ends to reduce the mode transform loss from the silicon waveguide to the SSHW. The SSHW mode then excites the two

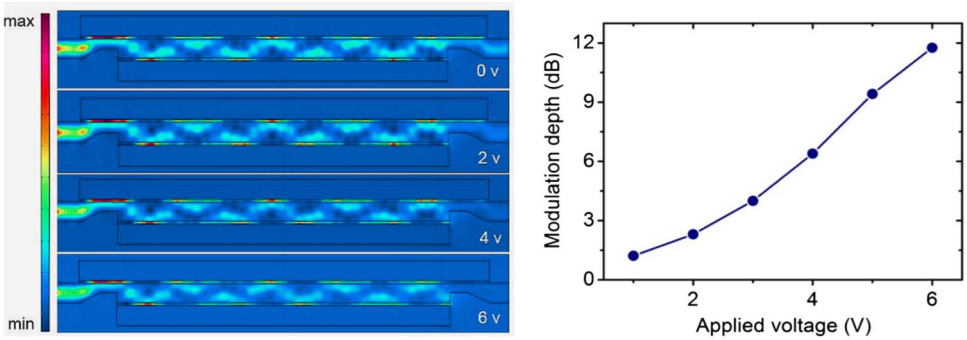

Fig. 6. (a) Optical power flow under various bias voltages. (b) Modulation depth changes as a function of voltage. The wavelength is set at 1550 nm.

super-modes of the DSHW. The two super-modes need to be nearly equally excited in order to achieve a high modulation depth. Here, we define the modulation depth as the ratio between the maximum and minimum output powers in response to a voltage

$$MD(dB) \equiv 10\lg\left(\frac{P_{out(\max)}}{P_{out(\min)}}\right). \tag{7}$$

Sensitivity, coupling length, and DSHW length all have significant influences on the modulation depth. A higher sensitivity S and a smaller coupling length L_c are favorable in improving the modulation depth and making the device compact. Considering the fabrication feasibility, we choose W_{si} and $W_{polymer}$ to be 450 nm and 50 nm, respectively. A long DSHW is beneficial to achieve a high modulation depth, but it suffers more propagation loss. The DSHW length L_3 is optimized to be 10.6 μm, allowing for a relatively high modulation depth and an acceptable insertion loss.

The SSHW silicon core width W_2 and length L_2 are the other two key parameters that affect the modulation depth. If the quasi-even and quasi-odd modes are excited equally, the optical power can be totally transferred from one slot to another, leading to a high modulation depth. In order to balance the excitation, the SSHW is designed to have dimensions of $L_2 = 510$ nm and $W_2 = 220$ nm where we get $C_{se} \approx C_{so}$.

In order to reduce the coupling loss between the silicon waveguide and the SSHW, the input/output taper length also needs to be optimized. There exists an optimal taper length where the back reflection loss and the metal absorption loss are compromised [32]. A longer taper has low back-reflection but suffers more metal absorption loss. The taper length L_1 is optimized to be 700 nm, giving rise to $\sim$1 dB coupling loss.

From the above analyses, the optimal structure is designed for relatively high modulation depth and bandwidth, acceptable propagation loss, and feasible fabrication. The optimal device geometric parameters are chosen as: $W_{si} = 450$ nm, $W_{polymer} = 50$ nm, $W_2 = 220$ nm, $L_1 = 700$ nm, $L_2 = 510$ nm, and $L_3 = 10.6$ μm. Fig. 6(a) shows the simulated optical power flow in the modulator under various applied voltages using the three-dimensional (3D) finite element method (FEM) simulation. The optical power coupled from the input silicon waveguide to the hybrid plasmonic waveguide travels in a zigzag path. It is finally coupled back to the silicon waveguide with the transmittance controlled by the applied voltage. There is no significant back reflection emanating from the open-end of the DSHW. Fig. 6(b) shows that the modulation depth changes with the applied voltage. The modulation depth reaches 12 dB with 6 V voltage (assuming $r_{33} = 200$ pm/V). The modulation efficiency of a Mach-Zehnder modulator is usually measured by the product $V_\pi \cdot L$. In our device, optical modulation is realized based on the coupling of hybrid plasmonic modes and V_π can be defined as the voltage swing to achieve the maximum modulation depth. The modulation depth approaches the maximum at 6 V, and therefore we have $V_\pi \approx 6$ V and $V_\pi \cdot L \approx 0.0078$ V $\cdot$ cm.

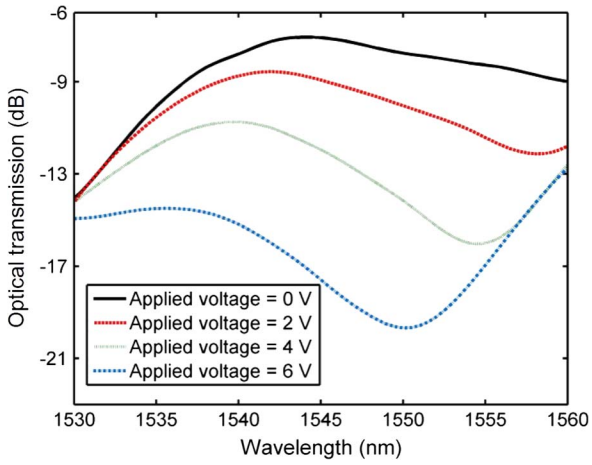

Fig. 7. Transmission spectra at various voltages.

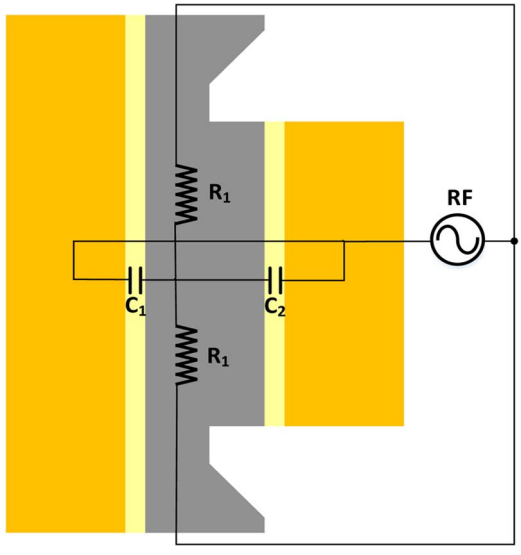

Fig. 8. Circuit model of the modulator.

Fig. 7 shows the transmission spectra under various voltages. At 1543 nm, the modulation depth is 10 dB at 6 V and the insertion loss is around 7 dB. The insertion loss is made up of ~1 dB propagation loss, ~1 dB photonic to SSHW mode transform loss per end, and ~2 dB SSHW to DSHW mode transform loss per end. At 1550 nm, the insertion loss is slightly increased to 7.7 dB, while the modulation depth reaches the maximum of 12 dB.

4.5. Modulation Speed and Power Consumption

Given that the inherent response time of the polymer is on the order of femtoseconds [33], the modulation speed of the device is mainly limited by the charging and discharging time (RC time) of the capacitor. Fig. 8 shows the equivalent circuit model of the device. The 3×10^{19} cm^{-3} n-type doping in the silicon strip lowers the silicon resistance to 2×10^{-3} ohm $\cdot$ cm. A radio frequency (RF) signal is applied between the metal and the silicon strip with a peak-to-peak voltage swing of V_{pp} and a bias of $V_{pp}/2$. As the modulator is relatively short, the electrode can be regarded as a lumped element, and the impedance matching is not taken into consideration. The total capacitance is $C = C_1 + C_2 = 2.7$ fF and the resistance is $R = R_1/2 = 660$ ohm. Note that R_1 is formed by the

doped silicon strip with a half-length of the modulator. It is overestimated in this rough estimation since the current density increases toward the ends of the modulator. The RC delay time is about 1.78 ps, corresponding to a modulation bandwidth of $f_{3\,dB} = 1/(2\pi RC) \approx 90$ GHz. The power consumption per bit is $1/4CV_{pp^2} = 24.3$ fJ/bit $(V_{pp} = 6\ V)$ [34], [35].

5. Conclusion

We proposed a novel optical intensity modulator based on a hybrid plasmonic waveguide consisting of Si-polymer-Ag layers. The optical field with TE polarization is strongly confined in the nanometer thin polymer layer. Due to the mode beating in the DSHW, the output power is dependent on the phase difference between the quasi-even and quasi-odd modes of the DSHW. Intensity modulation is realized by applying a voltage on the polymer layer, making use of its high linear EO effect. Several key parameters that determine the modulator performances were analyzed in detail. At 1550 nm, the modulation depth can reach 12 dB with a 6 V peak-to-peak voltage. Due to its compact size, the response time is about 1.78 ps, corresponding to a modulation bandwidth of 90 GHz. The power consumption is 24.3 fJ/bit. The high performance of the modulator can serve as a basic building block for future micro- and nano-scale plasmonic integrated circuits for optical signal processing and interconnect applications.

References

[1] G. T. Reed, G. Mashanovich, F. Y. Gardes, and D. J. Thomson, "Silicon optical modulators," *Nat. Photon.*, vol. 4, no. 8, pp. 518–526, Jul. 2010.

[2] Y. H. Kuo *et al.,* "Strong quantum confined Stark effect in germanium quantum-well structures on silicon," *Nature*, vol. 437, no. 27, pp. 1334–1336, Oct. 2005.

[3] Z. Y. Li *et al.,* "Silicon waveguide modulator based on carrier depletion in periodically interleaved PN junctions," *Opt. Exp.*, vol. 17, no. 18, pp. 15 947–15 958, Aug. 2009.

[4] J. F. Ding *et al.,* "Ultra-low-power carrier-depletion Mach-Zehnder silicon optical modulator," *Opt. Exp.*, vol. 20, no. 7, pp. 7081–7087, Mar. 2012.

[5] A. S. Liu *et al.,* "High-speed optical modulation based on carrier depletion in a silicon waveguide," *Opt. Exp.*, vol. 15, no. 2, pp. 660–668, Jan. 2007.

[6] R. A. Soref and B. R. Bennett, "Electrooptical effects in silicon," *IEEE J. Sel. Top. Quantum Electron.*, vol. JSTQE-23, no. 1, pp. 123–129, Jan. 1987.

[7] G. Cocorullo and I. Rendina, "Thermo-optical modulation at 1.5 μm in silicon etalon," *Electron. Lett.*, vol. 28, no. 1, pp. 83–85, Jan. 1992.

[8] M. T. Tinker and J. B. Lee, "Thermo-optic photonic crystal light modulator," *Appl. Phys. Lett.*, vol. 86, no. 22, pp. 22111-1–22111-3, May 2005.

[9] A. E. Willner and S. R. Nuccio, "Electro-optic polymer modulators," presented at the Opt. Fiber Commun. Conf., Los Angeles, CA, USA, 2012, Paper OW4F.1.

[10] P. Rabiei, W. H. Steier, C. Zhang, and L. R. Dalton, "Polymer microring filters and modulators," *J. Lightw. Technol.*, vol. 20, no. 11, pp. 1968–1975, Nov. 2002.

[11] V. M. Agranovich and D. L. Mills, *Surface Polaritons: Electromagnetic Waves at Surfaces and Interfaces*. Amsterdam, The Netherlands: Elsevier, 1982.

[12] A. Melikyan *et al.,* "High-speed plasmonic phase modulators," *Nat. Photon.*, vol. 8, no. 3, pp. 229–233, Mar. 2014.

[13] W. Shin *et al.,* "Broadband sharp 90-degree bends and T-splitters in plasmonic coaxial waveguides," *Nano Lett.*, vol. 13, no. 10, pp. 4753–4758, Oct. 2013.

[14] K. J. A. Ooi, P. Bai, H. S. Chu, and L. K. Ang, "Ultracompact vanadium dioxide dual-mode plasmonic waveguide electroabsorption modulator," *Nanophoton.*, vol. 2, no. 1, pp. 13–19, Feb. 2013.

[15] V. J. Sorger, N. D. Lanzillotti-Kimura, R.-M. Ma, and X. Zhang, "Ultra-compact silicon nanophotonic modulator with broadband response," *Nanophoton.*, vol. 1, no. 1, pp. 17–22, Jul. 2012.

[16] D. K. Gramotnev and S. I. Bozhevolnyi, "Plasmonics beyond the diffraction limit," *Nat. Photon.*, vol. 4, no. 2, pp. 83–91, Jan. 2010.

[17] D. F. P. Pile, D. K. Gramotnev, R. F. Oulton, and X. Zhang, "On long-range plasmonic modes in metallic gaps," *Opt. Exp.*, vol. 15, no. 21, pp. 13 669–13 674, Oct. 2007.

[18] R. F. Oulton, V. J. Sorger, D. A. Genov, D. F. P. Pile, and X. Zhang, "A hybrid plasmonic waveguide for subwavelength confinement and long-range propagation," *Nat. Photon.*, vol. 2, no. 8, pp. 496–500, Jul. 2008.

[19] D. X. Dai and S. L. He, "Low-loss hybrid plasmonic waveguide with double low-index nano-slots," *Opt. Exp.*, vol. 18, no. 17, pp. 17 958–17 966, Aug. 2010.

[20] X. M. Sun, L. J. Zhou, X. W. Li, Z. H. Hong, and J. P. Chen, "Design and analysis of a phase modulator based on a metal-polymer-silicon hybrid plasmonic waveguide," *Appl. Opt.*, vol. 50, no. 20, pp. 3428–3434, Jul. 2011.

[21] X. M. Sun *et al.,* "Miniature intensity modulator based on a silicon-polymer hybrid plasmonic waveguide," in *Proc. SPIE*, Feb. 2012, vol. 8333, p. 83330C.

[22] G. T. Reed and A. P. Knights, *Silicon Photonics: An Introduction*. Hoboken, NJ, USA: Wiley, 2004.

[23] J. Basak *et al.,* "Developments in gigascale silicon optical modulators using free carrier dispersion mechanisms," *Adv. Opt. Technol.*, vol. 2008, p. 678948, Apr. 1–10, 2008.
[24] T. B. Jones, B. Penkov, and J. Huang, "Nonlinear polymer-clad silicon slot waveguide modulator with a half wave voltage of 0.25 V," *Appl. Phys. Lett.*, vol. 92, no. 16, pp. 163303-1–163303-3, Apr. 2008.
[25] T. Nakano, K. Baba, and M. Miyagi, "Insertion loss and extinction ratio of a surface plasmon-polariton polarizer: Theoretical analysis," *J. Opt. Soc. Amer. B*, vol. 11, no. 10, pp. 2030–2035, Oct. 1994.
[26] A. Degiron, S. Y. Cho, T. Tyler, N. M. Jokerst, and D. R. Smith, "Directional coupling between dielectric and long-range plasmon waveguides," *N. J. Phys.*, vol. 11, no. 1, pp. 015002-1–015002-10, Jan. 2009.
[27] F. Lou, Z. C. Wang, D. X. Dai, L. Thylen, and L. Wosinski, "Experimental demonstration of ultra-compact directional couplers based on silicon hybrid plasmonic waveguides," *Appl. Phys. Lett.*, vol. 100, no. 24, pp. 241105-1–241105-4, Jun. 2012.
[28] H. Nejati and A. Beirami, "Theoretical analysis of the characteristic impedance in metal-insulator-metal plasmonic transmission lines," *Opt. Lett.*, vol. 37, no. 6, pp. 1050–1052, Mar. 2012.
[29] P. Johnson and R. Christy, "Optical constants of the noble metals," *Phys. Rev. B*, vol. 6, no. 12, pp. 4370–4379, Dec. 1972.
[30] T. D. Kim *et al.,* "Ultralarge and thermally stable electro-optic activities from supramolecular selfassembled molecular glasses," *J. Amer. Chem. Soc.*, vol. 129, no. 3, pp. 488–489, Jan. 2007.
[31] I. Avrutsky, R. Soref, and W. Buchwald, "Sub-wavelength plasmonic modes in a conductor-gap-dielectric system with a nanoscale gap," *Opt. Exp.*, vol. 18, no. 1, pp. 348–363, Jan. 2010.
[32] L. Chen, J. Shakya, and M. Lipson, "Subwavelength confinement in an integrated metal slot waveguide on silicon," *Opt. Lett.*, vol. 31, no. 14, pp. 2133–2135, Jul. 2006.
[33] L. R. Dalton *et al.,* "Organic electro-optic materials," in *Proc. SPIE*, Dec. 2004, vol. 5621, pp. 93–104.
[34] M. Ziebell *et al.,* "Ten Gbit/s ring resonator silicon modulator based on interdigitated PN junctions," *Opt. Exp.*, vol. 19, no. 15, pp. 14690–14695, Jul. 2011.
[35] M. R. Watts, D. C. Trotter, R. W. Young, and A. L. Lentine, "Ultralow power silicon microdisk modulators and switches," in *Proc. IEEE Int. Conf. Group IV Photon.*, 2008, pp. 4–6.